Neuron, Vol. 34, 821–830, May 30, 2002, Copyright ©2002 by Cell Press

Respiratory Rhythm: An Emergent Network Property?

Christopher A. Del Negro,[1]
Consuelo Morgado-Valle, and Jack L. Feldman
Systems Neurobiology Laboratory
Department of Neurobiology
University of California-Los Angeles
Box 95-1763
Los Angeles, California 90095

Summary

We tested the hypothesis that pacemaker neurons generate breathing rhythm in mammals. We monitored respiratory-related motor nerve rhythm in neonatal rodent slice preparations. Blockade of the persistent sodium current (I_{NaP}), which was postulated to underlie voltage-dependent bursting in respiratory pacemaker neurons, with riluzole (≤200 μM) did not alter the frequency of respiratory-related motor output. Yet, in every pacemaker neuron recorded (50/50), bursting was abolished at much lower concentrations of riluzole (≤20 μM). Thus, eliminating the pacemaker population (our statistics confirm that this population is reduced at least 94%, $p < 0.05$) does not affect respiratory rhythm. These results suggest that voltage-dependent bursting in pacemaker neurons is not essential for respiratory rhythmogenesis, which may instead be an emergent network property.

Introduction

Brain rhythms are widespread, essential for rhythmic movements, common during development, and may underlie important higher functions, including cognition. The bursting properties of pacemaker neurons are postulated to underlie many of these rhythms. Here, we test the hypothesis that pacemaker neurons with intrinsic voltage-dependent bursting properties generate the breathing rhythm in mammals (Ballanyi et al., 1999; Onimaru et al., 1997; Rekling and Feldman, 1998; Smith, 1997; Smith et al., 2000, 1991).

Normal breathing in intact adult rats requires neurons in the preBötzinger Complex (preBötC) (Gray et al., 2001), a specialized respiratory-related region of the ventral medulla (Rekling and Feldman, 1998). For the generation of respiratory-related motor rhythms in vitro, preBötC neural circuits are necessary and sufficient (Smith et al., 1991). Moreover, respiratory-related rhythm in vitro persists after blockade of chloride-mediated synaptic inhibition (Feldman and Smith, 1989; Onimaru et al., 1990), which suggests that neurons intrinsically able to produce periodic burst activity generate the rhythm. These data underlie the pacemaker hypothesis (q.v., Rekling and Feldman, 1998): preBötC voltage-dependent pacemaker neurons comprise the kernel for respiratory rhythm generation.

Pacemaker neurons are present in the preBötC (Del Negro et al., 2001; Johnson et al., 1994; Koshiya and Smith, 1999; Smith et al., 1991; Thoby-Brisson and Ramirez, 2001). Synaptically isolated preBötC pacemaker neurons generate repeating cycles of transient bursts of impulses separated by longer-lasting quiescent intervals, which are due to voltage-dependent membrane properties (Butera et al., 1999a; Thoby-Brisson and Ramirez, 2001). The frequency and duration of these cellular bursts are similar to the frequency and duration of the respiratory-related motor output generated by the intact network in vitro (Johnson et al., 1994). Predictions following from mathematical models of rhythmically active networks of voltage-dependent pacemaker neurons (Butera et al., 1999a, 1999b), when evaluated experimentally (Del Negro et al., 2001), also produce results consistent with the pacemaker hypothesis. Consequently, voltage-dependent pacemaker neurons are favored candidates for the critical respiratory rhythm-generating cells contained in the preBötC (Ballanyi et al., 1999; Koshiya and Smith, 1999; Rekling and Feldman, 1998; Richter and Spyer, 2001).

Here, we attempt to falsify the pacemaker hypothesis by testing its foremost prediction: if voltage-dependent pacemaker behavior is abolished in preBötC neurons, then respiratory rhythm should be severely perturbed, or even cease. We recorded from preBötC pacemaker neurons in neonatal rat and mouse medullary slice preparations at or prior to postnatal day (P)5 and monitored respiratory-related motor output via the hypoglossal nerve (XIIn) roots. Respiratory-modulated voltage-dependent pacemaker neurons in the preBötC depend on a persistent Na^+ current (I_{NaP}) for rhythmic burst generation (Del Negro et al., 2001; Johnson et al., 1994; Thoby-Brisson and Ramirez, 2001). Therefore, we used the Na^+ channel antagonist riluzole to selectively block I_{NaP} (Urbani and Belluzzi, 2000), which abolished bursting behavior in 50/50 preBötC pacemaker neurons tested. At concentrations of riluzole equal or much greater than necessary to block I_{NaP} and pacemaker activity, there was no effect on the frequency of respiratory-related motor output. This result challenges the validity of the pacemaker hypothesis based on voltage-dependent bursting properties and suggests that alternative neural mechanisms of respiratory rhythm generation, which do not depend on endogenous bursting properties of pacemaker neurons, must be considered.

Results

Respiratory Rhythm Persists following Bath Application of Riluzole

Riluzole was applied to slice preparations at concentrations from 1–200 μM in the presence of bicuculline and strychnine, which block chloride-mediated postsynaptic inhibition. Riluzole did not block respiratory-related motor output at these concentrations and did not change its mean frequency, although variability increased slightly at ascending doses (Figure 1). Riluzole reduced the magnitude of the XIIn motor output in a dose-dependent

[1]Correspondence: delnegro@ucla.edu

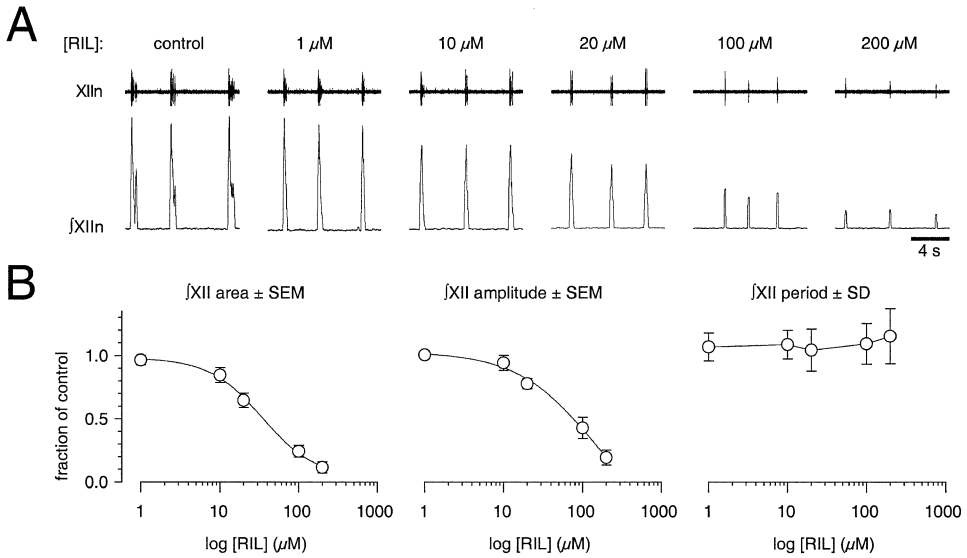

Figure 1. The Effects of Riluzole on Respiratory-Related Motor Output In Vitro

(A) Motor activity recorded from the hypoglossal nerve (XIIn) in a cumulative dose-response experiment. Riluzole concentration (RIL) is displayed above each trace. Raw and integrated traces (∫XIIn) are shown.

(B) Dose-response curves for ∫XIIn area, amplitude, and period (mean ± standard error [SEM] for area and amplitude and mean ± standard deviation [SD] for period; n = 16) are plotted versus riluzole concentration (RIL). The EC_{50} for area and amplitude effects are 33 and 48 μM, respectively. Riluzole had no systematic effect on respiratory period.

manner, which we quantified by measuring the amplitude and computing the area of the integrated nerve bursts; the EC_{50}s were 48 and 33 μM, respectively (Figure 1B; n = 16). These experiments were performed using ten mice and six rats. The dose-response curves for rat and mouse superimposed were statistically indistinguishable using the Kolmogorov-Smirnov 2-sample test for cumulative XIIn amplitude or area distributions ($p \approx 0.25$) and a t test for period ($p = 0.35$); thus, rodent samples were pooled. In four experiments, we simultaneously applied 10 μM nifedipine, which blocks L type Ca^{2+} channels (Fox et al., 1987a, 1987b) and 10 μM riluzole. The results were indistinguishable from experiments where 10 μM riluzole was applied alone (i.e., there was no effect on the mean frequency of respiratory-related motor output and no additional decline in XIIn activity) (data not shown). The significance of these unexpected results depends entirely on how riluzole affects pacemaker neurons.

Riluzole Blocks Bursting Behavior in Pacemaker Neurons

We recorded from pacemaker neurons to determine whether riluzole could prevent bursting via its selective blockade of I_{NaP} (Urbani and Belluzzi, 2000). Respiratory pacemaker neurons discharge in phase with XIIn motor rhythm (Figure 2A) but can be distinguished from non-pacemaker neurons by depolarizing baseline membrane potential, which causes pacemakers to generate ectopic bursts during the intervals between XIIn motor output (Figure 2B). Ectopic bursts occur in the absence of network-mediated burst activity and, thus, reflect the intrinsic voltage-dependent burst-generating mechanism, which is based on I_{NaP} (Del Negro et al., 2001). We synaptically isolated ectopic burst-generating neurons using low Ca^{2+} (0.5 mM)/high-Mg^{2+} (2 mM) artificial cerebrospinal fluid (ACSF) containing 100 μM Cd^{2+} (subsequently called low Ca^{2+} ACSF) (n = 45) or using normal ACSF with 5 μM CNQX (n = 5), which blocks postsynaptic ionotropic glutamate receptors that convey respiratory drive (Funk et al., 1993; Koshiya and Smith, 1999). After synaptic isolation, pacemaker neurons generated periodic bursting (Figure 2C). The bursts in low Ca^{2+} ACSF were qualitatively similar to the ectopic bursts produced in control (Figure 2B, inset) because I_{NaP} dominates the burst-generating mechanism (Del Negro et al., 2001; Johnson et al., 1994; Thoby-Brisson and Ramirez, 2001).

Riluzole (≤20 μM) blocked bursting in all 50 pacemaker neurons tested (Figures 2D and 3). We used bias current to slowly adjust membrane potential from −70 to −40 mV and search for baseline membrane potentials that might induce voltage-dependent intrinsic bursting. Slow continuous changes in bias current (Figure 2D), a series of small, step-like changes in bias current (Figure 3A), or slow, ramp-like commands (Figure 3B) were used. Without exception, bursting in preBötC pacemaker neurons was blocked by riluzole (n = 2 at 1 μM, n = 45 at 10 μM, and n = 3 at 20 μM).

Figures 1–3 suggest that voltage-sensitive pacemaker neurons are not required to generate respiratory rhythm in vitro. However, the strength of the conclusions that can be drawn from these results depends on whether there are other potentially confounding effects of riluzole on respiratory neurons and the extent to which riluzole abolished pacemaker activity in the entire rhythm-generating network.

Riluzole Effects on the Membrane Properties of Respiratory Neurons

To determine the effects of riluzole on I_{NaP} in respiratory neurons, we synaptically isolated neurons using low

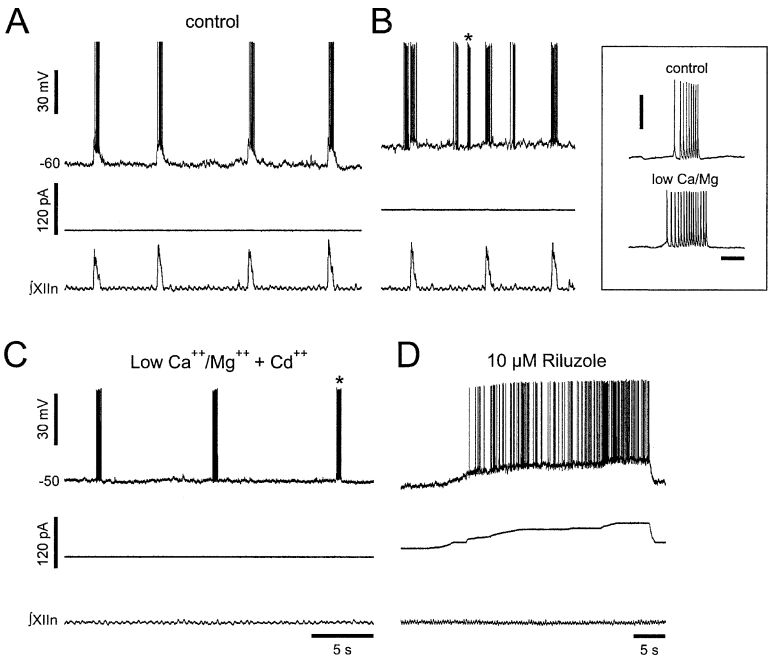

Figure 2. Riluzole Abolishes Voltage-Dependent Bursting Behavior in PreBötC Respiratory Pacemaker Neurons

(A) Respiratory-modulated discharge in a pacemaker neuron at its baseline resting membrane potential (top trace). Bias current (0 pA) is shown (middle trace). Respiratory network activity is shown via ∫XIIn motor output (bottom trace). Voltage and current calibration bars apply to (A) and (B).

(B) Respiratory-modulated discharge and "ectopic" bursts after depolarizing baseline membrane potential via current bias. Inset shows the ectopic burst (marked with the asterisk in [B]) and a spontaneous burst recorded in low Ca^{2+} ACSF (from [C]).

(C) Intrinsic bursting behavior in low Ca^{2+} ACSF, the asterisk denotes the burst expanded in (B) (inset). Respiratory network activity is blocked under these conditions; thus, ∫XIIn is silent (bottom trace). Time calibration bar in (C) applies to (A)–(C).

(D) 10 μM riluzole irreversibly blocked bursting behavior. A specific time calibration bar is shown.

Ca^{2+} ACSF with 10 mM tetraethylammonium (TEA). We recorded Na^+ currents in voltage-clamp with a Cs^+-based electrode solution (see Experimental Procedures). I_{NaP} was evoked by 20 mV/s descending (n = 11) or ascending (n = 4) ramp commands, which inactivate the fast Na^+ current responsible for action potentials but do not completely inactivate I_{NaP}. 20 μM riluzole greatly reduced I_{NaP} (Figure 4A). I_{NaP} (obtained by subtraction) activated near −60 mV and peaked at approximately −20 mV (57 ± 8 pA, n = 11 at 20 μM riluzole; Figure 4B). Riluzole antagonized I_{NaP} in a dose-dependent manner with an EC_{50} of 3 μM (Figure 4D, open circles).

Next, we examined the effects of riluzole on evoked action potentials. Spikes were triggered by 5 ms current steps (at rheobase) from a holding potential of −60 mV. Figure 4C (left) shows a cumulative dose-response experiment. Spike amplitude (measured from prestimulus baseline membrane potential to peak) decreased in a dose-dependent manner: amplitude declined ≤8% at riluzole concentrations ≤20 μM and declined no more than 31% at 200 μM, the highest concentration tested. The EC_{50} was 38 μM (Figure 4D, closed circles, n = 6). Spike threshold, rheobase, and action potential duration also increased in a dose-dependent manner in the presence of riluzole (Figure 4C, right). At 10 μM, the standard dose of riluzole to block pacemaker activity, spike threshold was generally 4 mV higher than control (see Figure 4C, open triangles). Action potentials were not blocked by riluzole at any concentration but were blocked by 1 μM tetrodotoxin (TTX, n = 4; data not shown).

We investigated the effects of riluzole on the membrane properties and repetitive spiking capabilities of respiratory neurons synaptically isolated in low Ca^{2+}

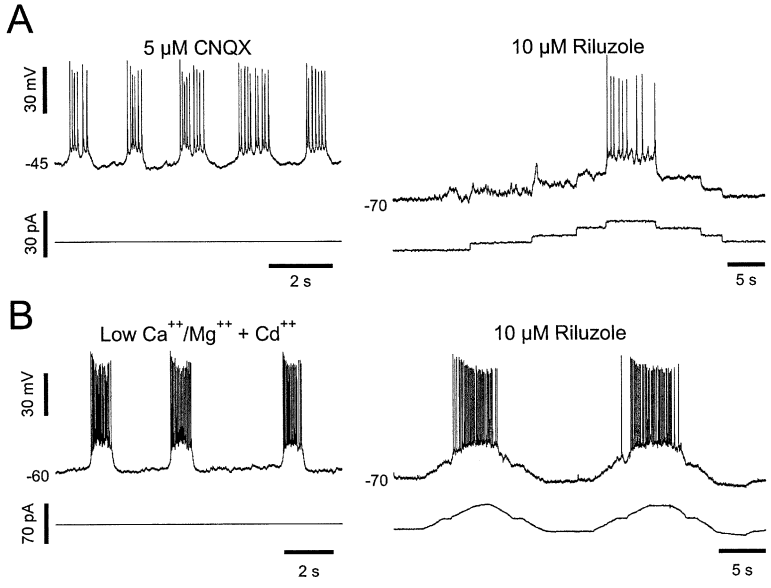

Figure 3. Examples of PreBötC Pacemaker Activity Blocked by Riluzole: Representative Examples Using Different Experimental Protocols

(A) Bursting in a pacemaker neuron synaptically isolated by 5 μM CNQX in normal ACSF. Small step changes in the current bias were used to probe for voltage-dependent bursting in the presence of 10 μM riluzole. Note that the left and right panels have separate time calibration bars.

(B) Bursting in a different pacemaker neuron isolated in low Ca^{2+} ACSF. Ascending and descending current ramps could not elicit bursting in the presence of 10 μM riluzole. Note that the left and right panels have separate time calibration bars.

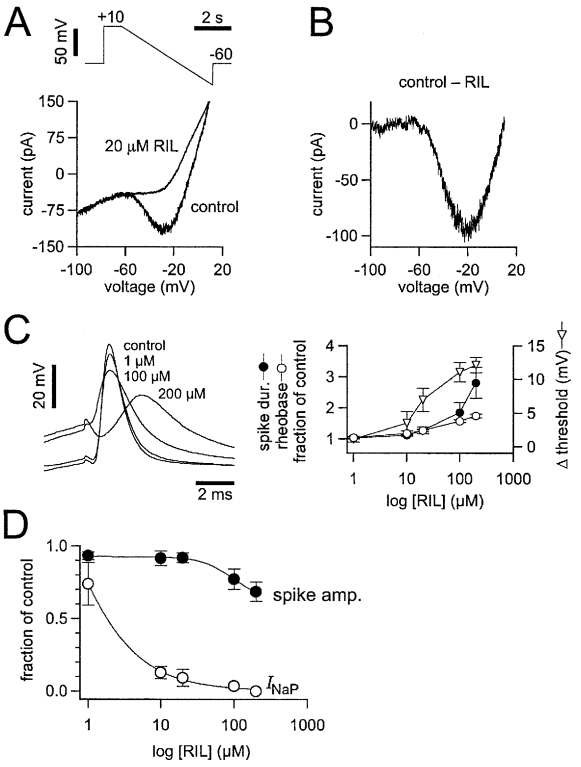

Figure 4. The Effects of Riluzole on I_{NaP} and Action Potentials in PreBötC Respiratory Neurons

(A) The current-voltage curves generated by descending voltage-ramps (top) in control and in the presence of 20 μM riluzole (RIL).
(B) The riluzole-sensitive current (from [A]) was obtained by subtraction, which represents I_{NaP}.
(C) Action potentials in a preBötC pacemaker neuron were evoked by 5 ms current stimuli (at rheobase) during a cumulative riluzole dose-response experiment (left). The baseline membrane potential was −60 mV for all traces (not shown). The dose-response curve (right) plots riluzole-induced changes in action potential duration (closed circles) and rheobase (open circles) plotted as fraction of control on the left axis, as well as riluzole-induced elevation of spike threshold (open triangles) in mV on the right axis.
(D) The dose-response curves show riluzole inhibition of spike amplitude (closed circles) and I_{NaP} (open circles). The EC_{50} for these effects is 38 and 3 μM, respectively.

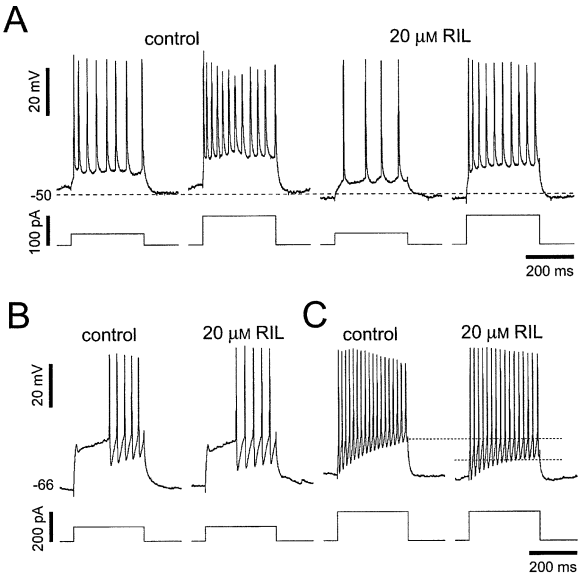

Figure 5. The Effects of Riluzole on Membrane Properties and Repetitive Spiking Behavior in PreBötC Neurons

(A) Membrane responses to 300 ms current step commands are shown for control conditions and in the presence of 20 μM riluzole (RIL). The resting membrane potential in this cell was hyperpolarized by 5 mV in the presence of riluzole (broken line for reference).
(B) The preBötC respiratory neuron shows delayed excitation in response to current-step commands. A bias current of −100 pA was applied to maintain baseline membrane potential at −66 mV in the presence and absence of riluzole.
(C) In another preBötC respiratory neuron, repetitive spike discharge results in response to larger-magnitude current stimuli. This neuron was maintained at the baseline membrane potential −55 mV (−40 pA holding current). 20 μM riluzole did not significantly change the frequency of the spikes evoked (bias current in riluzole was −20 pA). Current, voltage, and time calibrations apply to (B) and (C).

ACSF. Riluzole hyperpolarized the resting membrane potential by 1–5 mV at all concentrations tested and decreased the total number (and the frequency) of action potentials evoked by depolarizing step commands (Figure 5A, n = 11).

We then repeated the step-command protocols using bias current to adjust for riluzole-induced hyperpolarization and stabilize the baseline membrane potential. In control solution with neurons whose voltage was held at hyperpolarized potentials below the activation threshold for I_{NaP} (e.g., −66 mV in Figure 5B), step commands evoked a spike train after a 150 ms "delayed excitation" that characterizes an important class of respiratory neurons ("Type 1," Rekling et al., 1996). After applying 20 μM riluzole, the characteristic delayed excitation and spike output were unchanged (Figure 5B). When membrane potential was held at more positive levels (e.g., −55 mV in Figure 5C), riluzole did not affect the mean spike frequency evoked by depolarizing step commands, as assessed using standard frequency-current protocols (sample traces shown in Figure 5C; n = 4). However, riluzole did affect the trajectory of the overall membrane response. In control, action potentials appeared to ride on an underlying plateau that progressively depolarized the spike fast-afterhyperpolarization (fAHP) and produced a shunting effect, that gradually decreased spike amplitude (Figure 5C). The plateau-like response disappeared in 20 μM riluzole: spike fAHPs remained at relatively hyperpolarized levels (compare the dashed lines in Figure 5C), and spike amplitude did not decline as notably as in control. All of these effects are consistent with the selective blockade of a persistent inward current such as I_{NaP}.

Statistical and Physiological Limits

A definitive test of the pacemaker hypothesis requires that riluzole prevent voltage-dependent bursting in all the respiratory pacemaker neurons of the preBötC. The cellular data above demonstrate that 100% of the pacemaker neurons we recorded (50/50 cells) depend on I_{NaP} and lost their intrinsic bursting capabilities in the presence of riluzole (≤20 μM). These data agree with all previous reports, which also show that burst generation in preBötC pacemaker cells depends predominantly

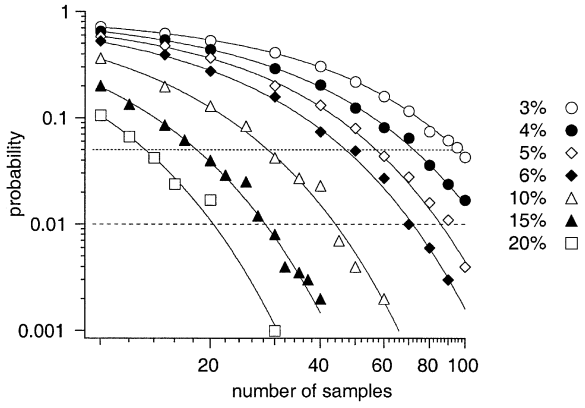

Figure 6. Monte Carlo Simulations of the PreBötC Pacemaker Neuron Sampling Protocol

The family of curves plot the probability of failing to find a single riluzole-insensitive pacemaker neuron for a sample size (n) represented on the abscissa if the hypothetical riluzole-insensitive cells actually comprise *x*% of the pacemaker population. Plots for several values of *x* are shown (3%–20%). Small and large dashed lines represent the 0.05 and 0.01 probability levels.

on I_{NaP} (Del Negro et al., 2001; Johnson et al., 1994; Thoby-Brisson and Ramirez, 2001). Nevertheless, this empirical sample represents a subset of all preBötC neurons and, if the idea that a separate subpopulation of previously and presently unidentified pacemaker neurons with a riluzole-insensitive voltage-dependent bursting mechanism exists, then what is the likelihood that we failed to uncover it?

We addressed this question statistically using Monte Carlo simulations. Our experimental protocol was simulated by sampling n times with replacement from a virtual urn containing *x*% white balls and (100 − *x*)% black balls (white balls symbolize riluzole-insensitive pacemakers; black balls symbolize riluzole-sensitive pacemakers). For several values of *x* (3%, 4%, 5%, 6%, 10%, 15%, and 20%) and n (10–200), we sampled repeatedly (Manly, 1991) to determine the probability (p) of finding only black balls (with ≥1000 trials for each value of *x* and n). Samples composed entirely of black balls became progressively unlikely as *x* (the percentage of white balls) and/or sample size (n) increased (Figure 6).

In our case with n = 50, failing to discover a single riluzole-insensitive pacemaker neuron was statistically unlikely ($p < 0.05$) if these neurons comprised ≥6% of the total pacemaker cell population (Figure 6). This statistically significant upper limit of undetected pacemaker neurons (<6%) overestimates the likely physiological upper limit, which may be 0%. Riluzole-insensitive pacemakers would have to utilize an ionic mechanism for bursting unrelated to voltage-dependent Na^+ (I_{NaP}) and Ca^{2+} currents, which are both antagonized by riluzole, albeit with different dose-dependence (Huang et al., 1997; Siniscalchi et al., 1997; Stefani et al., 1997; Urbani and Belluzzi, 2000), and could not depend on L type Ca^{2+} currents that are blocked by nifedipine (Fox et al., 1987a, 1987b) (see systems-level experiments above). Such pacemaker neurons have not been observed in the preBötC (Del Negro et al., 2001; Johnson et al., 1994; Koshiya and Smith, 1999; Thoby-Brisson and Ramirez, 2001). Therefore, riluzole-insensitive pacemakers probably do not exist in the preBötC (≤P5), and if so, then riluzole would eliminate all voltage-dependent pacemaker neuron behavior.

Controls

There are two other scenarios in which our riluzole experiments could fail to effectively test the pacemaker hypothesis. First, riluzole might fail to penetrate the tissue and, thus, fail to block the voltage-dependent bursting behavior of pacemaker cells located deep within the preBötC. Or, second, that the normal ACSF with 9 mM K^+ used in systems-level experiments engenders an alternative burst-generating mechanism in the presence of riluzole as an indirect effect of high K^+, thereby confounding the effects of riluzole to abolish voltage-dependent bursting.

To ensure that riluzole penetrated the standard slice preparation (400–550 μm thick), we repeated the dose-response experiments shown in Figure 1 using 350 μm (n = 4) and 750 μm (n = 3) slices. In all slices, XIIn motor output declined monotonically as the concentration of riluzole increased (as shown in Figure 1). In 750 μm slices, riluzole caused no change in the mean frequency of XIIn motor output at concentrations of 1–200 μM. In 350 μm thick slices, riluzole caused no change in the mean frequency at concentrations of 1–20 μM. However, at riluzole concentrations ≥100 μM, it was impossible to reliably measure the declining XIIn motor nerve bursts because of lower signal-to-noise ratios in thin slices, which retain less respiratory neural architecture, including fewer output XII motoneurons.

In one mathematical model (Rybak et al., 2001), elevated extracellular K^+ can induce burst activity by attenuating K^+ currents, which produces an inward "window" current for burst generation. Even though elevated K^+ is not required for bursting in respiratory pacemaker neurons (Del Negro et al., 2001), we tested whether bursting could be restored in pacemaker cells in the presence of riluzole by elevating the K^+ concentration. After blocking bursting behavior with 10 μM riluzole (in low Ca^{2+} ACSF), we increased the external K^+ from 3 to 9 mM but could not elicit voltage-dependent bursting at any baseline membrane potential (n = 6; data not shown).

Discussion

We tested the pacemaker hypothesis using an in vitro mammalian model of neural generation of respiratory activity. Riluzole selectively blocked I_{NaP}, the burst-generating current in preBötC respiratory neurons, and, at concentrations ≤20 μM, abolished voltage-dependent bursting behavior in all 50 preBötC pacemaker neurons tested. Notably, riluzole at concentrations up to 10-fold higher did not prevent rhythm generation at the systems level, and in particular, did not alter its frequency. These results suggest that neither I_{NaP} nor the voltage-dependent bursting it engenders are essential for rhythm generation in thin medullary slices from neonatal rodents (P0–P4 rats and P1–P5 mice). The possibility that respiratory rhythm is an emergent network property, e.g., a "group-pacemaker" (Rekling and Feldman, 1998) or has

its cellular basis in a biochemical oscillation that does not require voltage-dependent bursting (Baker et al., 1995), warrants renewed consideration.

Effects of Riluzole on Respiratory Motor Nerve Output

The mean frequency of respiratory output was not affected by riluzole (≤200 μM), but its variability generally increased at higher concentrations (note: SD for period increases at ≥20 μM riluzole; Figure 1B). Therefore, the cellular properties blocked by riluzole may contribute to regular periodic network activity, even though they are not essential. Also, the area and the amplitude of the XIIn motor bursts declined as the riluzole concentration increased. The EC_{50} for the area and amplitude effects were 33 and 48 μM, respectively, which resembles the dose-dependent inhibition of spike amplitude by riluzole (EC_{50} = 38 μM, Figure 4D). Based on the similarity of these dose-dependent effects at the cellular and systems levels, the decline in motor output probably results from riluzole antagonism of spike amplitude in all respiratory neurons, including XII motoneurons (Umemiya and Berger, 1995). There are other effects of riluzole that may contribute to the decline in motor output as well as increase the cycle-to-cycle variability in respiratory period: riluzole inhibits high-threshold I_{Ca} (Huang et al., 1997; Siniscalchi et al., 1997; Stefani et al., 1997) and also activates nongated "leakage" K^+ currents (Duprat et al., 2000). All of these effects (decreased spike amplitude, reduced I_{Ca}, and the activation of passive K^+ conductances) may cause widespread depression of neural excitability. Lastly, riluzole may be toxic at doses exceeding 100 μM (Xu et al., 2001). That these other effects occur makes it all the more remarkable that respiratory-related motor output persists with unchanged mean frequency in the presence of riluzole.

Cellular Effects of Riluzole

Riluzole at concentrations <10 μM blocks I_{NaP} (Urbani and Belluzzi, 2000) without abolishing action potentials (Siniscalchi et al., 1997; Song et al., 1997; Stefani et al., 1997; Umemiya and Berger, 1995). In voltage-clamp, I_{NaP} activated in respiratory neurons at subthreshold voltages and was blocked by similarly low doses of riluzole (EC_{50} = 3 μM). In current-clamp, riluzole blocked an inward current active at rest that contributed to plateau-like responses when further evoked by membrane depolarization, which is also consistent with antagonism of I_{NaP}. In pacemaker neurons, riluzole abolished voltage-dependent bursting. Riluzole never blocked action potential generation but progressively decreased spike amplitude, prolonged spike duration, and increased threshold voltage as its concentration increased up to 200 μM (Figures 4C and 4D). Aside from its effects on I_{NaP}, riluzole also inhibits high-threshold Ca^{2+} channels of the N, P/Q, and R types (Huang et al., 1997; Siniscalchi et al., 1997; Stefani et al., 1997). Therefore, if I_{Ca} contributes to burst generation in some pacemaker neurons (even if the role of I_{Ca} is not essential), then riluzole would antagonize bursting by simultaneously blocking I_{NaP} (which is nearly complete at riluzole concentrations >10 μM) and substantially reducing I_{Ca}. We did not identify any pacemaker neurons that required I_{Ca} for burst generation since all the neurons that generated ectopic bursts in control ACSF continued bursting in low Ca^{2+} ACSF, as previously shown (Del Negro et al., 2001; Johnson et al., 1994). Nevertheless, a subset of respiratory pacemaker neurons that can be antagonized using either divalent cations, such as Cd^{2+} (≥50 μM) or TTX (0.5 μM) has recently been identified in thick-slice preparations from older postnatal mice (P6–P13) (Thoby-Brisson and Ramirez, 2001). We expect that bursting in these Cd^{2+}-sensitive pacemaker cells would also be antagonized by appropriate doses of riluzole because the drug suppresses both burst-generating currents I_{NaP} and I_{Ca}, and blockade of either intrinsic current is sufficient to abolish bursting (Thoby-Brisson and Ramirez, 2001). The Cd^{2+}-sensitive pacemakers appear to be developmentally regulated and may not exist in slice preparations (such as ours) taken at or prior to P5 (Thoby-Brisson and Ramirez, 2001).

Could I_{NaP}-Independent Pacemaker Neurons Exist in the PreBötC?

Is there an anomalous population of pacemaker cells employing a I_{NaP}-independent ionic mechanism in the presence of riluzole that could potentially operate as the kernel for respiratory rhythm generation?

L type I_{Ca} is the only subtype of I_{Ca} not antagonized by riluzole (Huang et al., 1997). We tested the possibility that L type I_{Ca}-dependent pacemakers underlie rhythm generation by applying nifedipine, which blocks the L type I_{Ca} (Fox et al., 1987a, 1987b) plus riluzole in systems-level experiments. The results were identical to experiments where riluzole was applied alone, suggesting that there was no significant L type I_{Ca} bursting activity essential for rhythm generation in the presence of riluzole.

We sampled pacemaker cells from both the rostral and caudal faces of our slices at depths of up to 120 μm in the preBötC. Although we were not able to record cells under visual control at depths exceeding 120 μm, our present finding that I_{NaP} dominates the burst-generating mechanism is corroborated by published studies that used "blind" recording techniques, which sample preBötC neurons at any depth (Del Negro et al., 2001; Johnson et al., 1994; Thoby-Brisson and Ramirez, 2001). This suggests that we obtained a representative sample of all pacemaker cells distributed throughout the preBötC of neonatal rodents (≤P5). Moreover, riluzole did not affect the frequency of motor output in both thinner or thicker slices (350 versus 750 μm), which indicates that riluzole readily penetrated the thicker preparations to act on cells at any depth.

Was our sample size too small to substantiate a negative result? Based on our statistics, the sample size was sufficiently large enough that the probability of failing to find a single riluzole-insensitive pacemaker neuron was less than 0.05, if such heretofore unseen neurons comprise ≥6% of the total pacemaker population. Therefore, if anomalous riluzole-insensitive pacemaker cells exist, then their statistically significant upper limit is small (less than 6% of all pacemaker neurons). Furthermore, such neurons would have to employ an unorthodox ionic bursting mechanism, since rhythmic activity that depends on I_{NaP} (Urbani and Belluzzi, 2000), as well as N, P/Q, or R type I_{Ca} (Huang et al., 1997; Siniscal-

chi et al., 1997; Stefani et al., 1997), is antagonized by riluzole, and our nifedipine experiments rule out bursting activity due to L type I_{Ca}. Finally no other laboratory has reported I_{NaP}-independent pacemaker neurons either (Del Negro et al., 2001; Johnson et al., 1994; Thoby-Brisson and Ramirez, 2001), which suggests that these anomalous pacemakers probably do not exist in the preBötC of early postnatal rodents.

Assessing the Pacemaker Hypothesis

To reject the hypothesis that the voltage-dependent bursting properties of pacemaker neurons comprise the kernel for respiratory rhythm generation, it is necessary to show that these specialized membrane properties are not required for rhythmogenesis.

Riluzole eliminated voltage-dependent bursting in all the preBötC pacemaker neurons we identified and caused no change in the frequency of respiratory-related motor output. Based on the statistical and physiological arguments above, riluzole probably abolished all voltage-dependent bursting behavior in preBötC neurons in the thin medullary slice preparation.

In the unlikely case that an anomalous population of I_{NaP}-independent pacemaker neurons exists in the presence of riluzole, then its size limitation ($<6\%$ of the original pacemaker population) puts an enormous constraint on the pacemaker hypothesis, requiring it to be formulated in a way that a small number of neurons could generate rhythmic activity with no change in frequency. We have used large-scale simulations to verify that this is impossible in several mathematical models of pacemaker networks. In the voltage-dependent pacemaker-network model by Butera and colleagues (1999b) (Del Negro et al., 2001), the network frequency decreases monotonically with reductions of I_{NaP}, which effectively reduces the number of pacemaker neurons participating in rhythm generation (C.A. Del Negro, unpublished data). Thus, in the model, output frequency is linked to I_{NaP} and the size of the pacemaker population, which is inconsistent with the present experiments where riluzole blocked I_{NaP} yet had no effect on the frequency.

If no bursting in voltage-dependent pacemaker neurons remains in the presence of riluzole, could the pacemaker hypothesis still be viable? Appropriately formulated, a mathematical model (Butera et al., 1999b) can generate respiratory-like rhythm when no constituent neurons are pacemakers, as defined by voltage-dependent bursting in the isolated cell (Koshiya and Smith, 1999; Rekling and Feldman, 1998; Smith et al., 1991; Thoby-Brisson and Ramirez, 2001). Rhythmicity in the coupled-model network can occur when I_{NaP} is decreased 42% throughout the network, which precludes intrinsic cellular bursting (Butera et al., 1999a), only if excitatory synaptic transmission is strengthened 2-fold or more to compensate for the reduction in I_{NaP}. Then, synchronized bursts initiate due to network-wide mutual synaptic excitation among constituent neurons but still terminate due to I_{NaP} inactivation, which causes cells to slowly hyperpolarize and, ultimately, terminate their spiking.

This mechanism is not likely to explain our results. First, it requires significantly elevated excitatory synaptic strength. We found no evidence for increased synaptic strength after riluzole application: respiratory drive potentials decreased in the presence of riluzole by 5%–27% (data not shown). This is consistent with previous reports showing that riluzole can depress, but not enhance, excitatory synaptic transmission (Cheramy et al., 1992; Debono et al., 1993; Jehle et al., 2000; Martin et al., 1993; Mizoule et al., 1985). Second, the termination of network burst activity in the model requires substantial I_{NaP} inactivation (Butera et al., 1999b). If I_{NaP} is eliminated altogether in the model, rhythmicity in the network is impossible. Here, we recorded respiratory-related rhythms at riluzole concentrations as high as 200 μM, and our cellular dose-response data shows I_{NaP} is virtually eliminated at low concentrations ($EC_{50} = 3$ μM, Figure 4D). Therefore, at riluzole doses >20 μM, it is very unlikely that sufficient I_{NaP} was present in constituent neurons to participate in rhythm generation.

We conclude that present models of rhythm generation in vitro, which are based on the pacemaker hypothesis and the voltage-dependence and kinetics of I_{NaP} (Butera et al., 1999b; Del Negro et al., 2001; Rekling and Feldman, 1998; Smith, 1997; Smith et al., 1992), cannot account for our results.

Emergent Mechanisms of Rhythm Generation

An emergent network-based mechanism for rhythm generation must be considered as an alternative to the pacemaker hypothesis. Rekling and Feldman (1998) proposed that the fundamental unit of oscillation could be an ensemble of neurons with similar or complementary intrinsic properties that become rhythmically active through chemical and electrotonic excitatory synaptic interactions (Rekling et al., 2000). This ensemble could then act as a "group pacemaker" for the respiratory rhythm. Until now, the attention regarding how rhythmogenic neurons interact in the network has focused exclusively on fast excitatory transmission mediated by ionotropic glutamate receptors (Funk et al., 1993; Ge and Feldman, 1998; Koshiya and Smith, 1999). We propose that the phasic activation of metabotropic glutamate receptors or the action of glutamate transporters could also influence periodic respiratory-related activity in the preBötC.

The original notion of a respiratory pacemaker did not require voltage-dependent bursting per se (Feldman and Smith, 1989). Respiratory-related rhythm in vitro may yet have a cellular pacemaker kernel, but the oscillatory process in these cells may be biochemical in nature. For example, autonomous intracellular Ca^{2+} oscillations, Ca^{2+}-activated Ca^{2+}-release cycles (Baker et al., 1995), Ca^{2+}-activated cationic currents (Rekling and Feldman, 1997b), or metabotropic receptor-mediated second-messenger systems could provide pacemaker-like rhythms in lieu of voltage-dependent bursting.

Propriobulbar respiratory neurons that express the neurokinin-1 receptor (NK-1R) delineate the anatomical boundaries of the preBötC in rats (Gray et al., 1999; Wang et al., 2001). Selective lesion of these NK-1R-expressing neurons results in ataxic pathological breathing patterns in intact adult rats (Gray et al., 2001). Neurons with voltage-dependent bursting properties are a subset of the NK-1R-expressing cells in the preBötC.

Therefore, pacemaker neurons may comprise a subset of the critical rhythm-generating population in the preBötC, but not because of their voltage-dependent bursting behavior per se.

We do not yet understand how closely the mechanism of rhythm generation in vitro represents that in behaving mammals, at any age. Postnatal developmental changes in networks generating respiratory rhythm may occur, but they must be seamless since they cannot significantly interrupt breathing. Changes in intracellular chloride concentration have been reported in preBötC neurons in rodents in the early postnatal period (P0–P5) (Ritter and Zhang, 2000). This could result in depolarizing (instead of hyperpolarizing) postsynaptic potentials in response to synaptic release of GABA and glycine during the first few days of life. Whether these changes occur and whether they specifically affect neurons in the rhythm-generating networks of the preBötC is controversial (Brockhaus and Ballanyi, 1998; Shao and Feldman, 1997). Moreover, even if E_{Cl} does shift during P0–P5, it does not affect our conclusions because in our systems-level experiments (see Figure 1), chloride currents were blocked by bicuculline and strychnine, which antagonize the GABA and glycine receptors that open chloride channels. There may also be postnatal changes in Ca^{2+} channel expression, which could explain the emergence of the Cd^{2+}-sensitive pacemaker neurons after P6 in mice (Thoby-Brisson and Ramirez, 2001) (also see above). Since our experiments were done on rodents P0–P5, the later observations would neither impact our findings nor our conclusions.

In addition, there are respiratory neurons in the brainstem that are not captured in thin slice preparations and may contribute to breathing patterns in vivo. In particular, neurons with pre-inspiratory (pre-I) discharge patterns are present in the ventral medulla, just rostral to the preBötC in en bloc brainstem-spinal cord preparations (Onimaru et al., 1989; Onimaru et al., 1997). Some pre-I neurons express pacemaker properties and are not contained in slice preparations; thus, we cannot evaluate how they contribute to rhythm generation in more intact states.

Experimental Procedures

Experiments were performed in vitro using rats ages P0–P4 and mice ages P1–P5. All protocols were approved by the Office for the Protection of Research Subjects, University of California Animal Research Committee. Rodents were anesthetized by hypothermia and dissected in normal ACSF containing: 124 mM NaCl, 3 mM KCl, 1.5 mM $CaCl_2$, 1 mM $MgSO_4$, 25 mM $NaHCO_3$, 0.5 mM NaH_2PO_4, and 30 mM D-glucose and equilibrated with 95% O_2 and 5% CO_2 (27°C) (pH = 7.4). Transverse medullary slices (400–550 μm thick) containing the preBötC were cut from the brainstem-spinal cord.

Slices were anchored in a 500 μl recording chamber (Warner Instruments GLP-26, www.warnerinstruments.com) using a platinum frame and a grid of nylon fibers (Edwards et al., 1989). The chamber was mounted to a fixed-stage microscope (Leica VM LFS-1, www.leica.com) and perfused with ACSF at 4 ml/min. Rhythmic respiratory-related motor output was recorded from the hypoglossal nerve roots (XIIn), which contain the axons of respiratory motoneurons also contained in the slice, using fire-polished glass suction electrodes, a differential amplifier (Grass Instruments, www.grassinstruments.com), and a 300–1000 Hz bandpass filter. We elevated the K^+ concentration to 9 mM in normal ACSF to obtain a robust and stable rhythm. XIIn activity was rectified and smoothed using analog integration (∫XIIn).

Low Ca^{2+} ACSF was used to block chemical synaptic transmission and suppress respiratory network activity during intracellular recordings. This solution contained: 124.5 mM NaCl, 3 mM KCl, 0.5 mM $CaCl_2$, 2 mM $MgCl_2$, 25 mM $NaHCO_3$, 30.0 mM D-glucose, and 100 μM $CdCl_2$. 10 mM TEA was substituted on a equimolar basis for NaCl to attenuate K^+ currents during voltage-clamp experiments. Drugs obtained from Sigma Chemical (www.sigma.com) were bath-applied at the following concentrations: 1–200 μM riluzole (2-amino-6-trifluoromethoxy benzothiazole), 1 μM TTX, 10 μM nifedipine, 5 μM CNQX (6-cyano-7-nitroquinoxaline-2,3-dione), 2–5 μM bicuculline, and 2–5 μM strychnine.

Respiratory neurons were visualized using infrared-enhanced differential interference contrast videomicroscopy (Inoué and Spring, 1997). Inspiratory cells generally had large triangle-shaped cell bodies and were located ventral to the semicompact division of the nucleus ambiguous—an easily recognized dense cluster of small, oval-shaped cells in the ventrolateral region of the slice (Rekling and Feldman, 1997a). We sampled respiratory neurons bilaterally from the left and right halves of the preBötC and from both the rostral and caudal surfaces of the slice preparation at depths of ≤120 μm. Whole-cell patch-clamp recordings were performed using Axoclamp-2A and Axopatch-200 amplifiers for current- and voltage-clamp experiments, respectively (Axon Instruments, www.axon.com). Electrodes were fabricated from capillary glass (O.D., 1.5 mm; I.D., 0.87 mm) in multistage programs on a Sutter Instruments P-97 Puller (www.sutterinstruments.com). For current-clamp experiments, electrodes were filled with solution containing: 140 mM K-gluconate, 5 mM NaCl, 10 mM HEPES, 2 mM Mg-ATP, and 0.3 mM Na_3-GTP (pH = 7.3). A liquid junction potential of +8 mV was corrected offline. Series resistance (R_S) was compensated via bridge balance. For voltage-clamp experiments, electrodes were filled with solution containing: 140 mM CsCl, 9 mM NaCl, 10 mM HEPES, 2 mM Mg-ATP, and 0.3 mM Na_3-GTP (pH = 7.3), which was used to attenuate K^+ currents and the hyperpolarization-activated mixed-cationic current I_h. The Cs^+-based patch solution increases the membrane resistance, which improves voltage-clamp fidelity at the pipette tip and extends voltage control spatially to more distal somatic regions and dendrites by making cells more electrotonically compact.

Input resistance (R_N) was determined from the current-voltage relationship generated by slow voltage-ramp commands (~10 mV/s) in the linear region negative to −50 mV. Cell capacitance (C_M) was determined from the integral of the transient capacity current (I_C, leak subtracted) evoked by 15 ms hyperpolarizing voltage-steps (ΔV_M), using the formula $C_M = \int I_C / \Delta V_M$. R_S was then calculated from the decay-time constant (τ) of I_C since $\tau \approx R_S \times C_M$ in voltage clamp, where τ is the estimated exponential I_C decay time. An acceptable voltage clamp requires $R_N \geq 10 \times R_S$. Cells failing to meet this criterion were discarded. R_S averaged 26 ± 4 MΩ (n = 18) and was compensated to 18 ± 2 MΩ (n = 10) via analog feedback. R_S compensation was applied without whole-cell capacity compensation in order to continuously monitor τ and ensure stationary voltage-clamp conditions.

Electrophysiological signals were acquired digitally at 4–20 kHz using pCLAMP software (Axon Instruments) after low-pass filtering. Igor Pro (Wave Metrics, www.wavemetrics.com), Chart (ADInstruments, www.adinstruments.com), and Microsoft excel (www.microsoft.com) were used for data analyses. Randomization and Monte Carlo statistical tests were performed using custom routines in Resampling Statistics (www.resample.com). Simulations of ordinary differential equation mathematical models (Butera et al., 1999a, 1999b; Del Negro et al., 2001) were performed using UC Berkeley's Madonna (www.berkeleymadonna.com) with an adjustable time step and stiff integrator with low error tolerance (10^{-6}).

Acknowledgments

The work was supported by NIH Grant HL-40959. C.A. Del Negro is a Parker B. Francis Fellow in Pulmonary Research (Francis Families Foundation, Kansas City, Missouri). We thank Paul Gray, Tom Otis, Jens Rekling, and Felix Schweitzer for helpful comments on the manuscript.

Received: December 20, 2001
Revised: April 18, 2002

References

Baker, R.E., Ballantyne, D., Bingmann, D., Jones, D., and Widman, G. (1995). Rhythm generation in organotypic medullary cultures of newborn rats. Int. J. Dev. Neurosci. *13*, 799–809.

Ballanyi, K., Onimaru, H., and Homma, I. (1999). Respiratory network function in the isolated brainstem-spinal cord of newborn rats. Prog. Neurobiol. *59*, 583–634.

Brockhaus, J., and Ballanyi, K. (1998). Synaptic inhibition in the isolated respiratory network of neonatal rats. Eur. J. Neurosci. *10*, 3823–3839.

Butera, R.J., Jr., Rinzel, J., and Smith, J.C. (1999a). Models of respiratory rhythm generation in the pre-Botzinger complex. I. Bursting pacemaker neurons. J. Neurophysiol. *82*, 382–397.

Butera, R.J., Jr., Rinzel, J., and Smith, J.C. (1999b). Models of respiratory rhythm generation in the pre-Botzinger complex. II. Populations of coupled pacemaker neurons. J. Neurophysiol. *82*, 398–415.

Cheramy, A., Barbeito, L., Godeheu, G., and Glowinski, J. (1992). Riluzole inhibits the release of glutamate in the caudate nucleus of the cat in vivo. Neurosci. Lett. *147*, 209–212.

Debono, M.W., Le Guern, J., Canton, T., Doble, A., and Pradier, L. (1993). Inhibition by riluzole of electrophysiological responses mediated by rat kainate and NMDA receptors expressed in Xenopus oocytes. Eur. J. Pharmacol. *235*, 283–289.

Del Negro, C.A., Johnson, S.M., Butera, R.J., and Smith, J.C. (2001). Models of respiratory rhythm generation in the pre-Bötzinger complex. III. Experimental tests of model predictions. J. Neurophysiol. *86*, 59–74.

Duprat, F., Lesage, F., Patel, A.J., Fink, M., Romey, G., and Lazdunski, M. (2000). The neuroprotective agent riluzole activates the two P domain K(+) channels TREK-1 and TRAAK. Mol. Pharmacol. *57*, 906–912.

Edwards, F.A., Konnerth, A., Sakmann, B., and Takahashi, T. (1989). A thin slice preparation for patch clamp recordings from neurones of the mammalian central nervous system. Pflugers Arch. *414*, 600–612.

Feldman, J.L., and Smith, J.C. (1989). Cellular mechanisms underlying modulation of breathing pattern in mammals. Ann. N. Y. Acad. Sci. *563*, 114–130.

Fox, A.P., Nowycky, M.C., and Tsien, R.W. (1987a). Kinetic and pharmacological properties distinguishing three types of calcium currents in chick sensory neurones. J. Physiol. (Lond.) *394*, 149–172.

Fox, A.P., Nowycky, M.C., and Tsien, R.W. (1987b). Single-channel recordings of three types of calcium channels in chick sensory neurones. J. Physiol. (Lond.) *394*, 173–200.

Funk, G.D., Smith, J.C., and Feldman, J.L. (1993). Generation and transmission of respiratory oscillations in medullary slices: role of excitatory amino acids. J. Neurophysiol. *70*, 1497–1515.

Ge, Q., and Feldman, J.L. (1998). AMPA receptor activation and phosphatase inhibition affect neonatal rat respiratory rhythm generation. J. Physiol. (Lond.) *509*, 255–266.

Gray, P.A., Rekling, J.C., Bocchiaro, C.M., and Feldman, J.L. (1999). Modulation of respiratory frequency by peptidergic input to rhythmogenic neurons in the preBötzinger complex. Science *286*, 1566–1568.

Gray, P.A., Janczewski, W.A., Mellen, N., McCrimmon, D.R., and Feldman, J.L. (2001). Normal breathing requires preBotzinger complex neurokinin-1 receptor-expressing neurons. Nat. Neurosci. *4*, 927–930.

Huang, C.S., Song, J.H., Nagata, K., Yeh, J.Z., and Narahashi, T. (1997). Effects of the neuroprotective agent riluzole on the high voltage-activated calcium channels of rat dorsal root ganglion neurons. J. Pharmacol. Exp. Ther. *282*, 1280–1290.

Inoué, S., and Spring, K.R. (1997). Video microscopy: The Fundamentals, Second Edition (New York: Plenum).

Jehle, T., Bauer, J., Blauth, E., Hummel, A., Darstein, M., Freiman, T.M., and Feuerstein, T.J. (2000). Effects of riluzole on electrically evoked neurotransmitter release. Br. J. Pharmacol. *130*, 1227–1234.

Johnson, S.M., Smith, J.C., Funk, G.D., and Feldman, J.L. (1994). Pacemaker behavior of respiratory neurons in medullary slices from neonatal rat. J. Neurophysiol. *72*, 2598–2608.

Koshiya, N., and Smith, J.C. (1999). Neuronal pacemaker for breathing visualized in vitro. Nature *400*, 360–363.

Manly, B.F.J. (1991). Randomization and Monte Carlo Methods in Biology, First Edition (London: Chapman and Hall).

Martin, D., Thompson, M.A., and Nadler, J.V. (1993). The neuroprotective agent riluzole inhibits release of glutamate and aspartate from slices of hippocampal area CA1. Eur. J. Pharmacol. *250*, 473–476.

Mizoule, J., Meldrum, B., Mazadier, M., Croucher, M., Ollat, C., Uzan, A., Legrand, J.J., Gueremy, C., and Le Fur, G. (1985). 2-Amino-6-trifluoromethoxy benzothiazole, a possible antagonist of excitatory amino acid neurotransmission—I. Anticonvulsant properties. Neuropharmacology *24*, 767–773.

Onimaru, H., Arata, A., and Homma, I. (1989). Firing properties of respiratory rhythm generating neurons in the absence of synaptic transmission in rat medulla in vitro. Exp. Brain Res. *76*, 530–536.

Onimaru, H., Arata, A., and Homma, I. (1990). Inhibitory synaptic inputs to the respiratory rhythm generator in the medulla isolated from newborn rats. Pflugers Arch. *417*, 425–432.

Onimaru, H., Arata, A., and Homma, I. (1997). Neuronal mechanisms of respiratory rhythm generation: an approach using in vitro preparation. Jpn. J. Physiol. *47*, 385–403.

Rekling, J.C., and Feldman, J.L. (1997a). Bidirectional electrical coupling between inspiratory motoneurons in the newborn mouse nucleus ambiguus. J. Neurophysiol. *78*, 3508–3510.

Rekling, J.C., and Feldman, J.L. (1997b). Calcium-dependent plateau potentials in rostral ambiguus neurons in the newborn mouse brain stem in vitro. J. Neurophysiol. *78*, 2483–2492.

Rekling, J.C., and Feldman, J.L. (1998). PreBötzinger complex and pacemaker neurons: hypothesized site and kernel for respiratory rhythm generation. Annu. Rev. Physiol. *60*, 385–405.

Rekling, J.C., Champagnat, J., and Denavit, S.M. (1996). Electroresponsive properties and membrane potential trajectories of three types of inspiratory neurons in the newborn mouse brain stem in vitro. J. Neurophysiol. *75*, 795–810.

Rekling, J.C., Shao, X.M., and Feldman, J.L. (2000). Electrical coupling and excitatory synaptic transmission between rhythmogenic respiratory neurons in the PreBotzinger complex. J. Neurosci. *20*, RC113.

Richter, D.W., and Spyer, K.M. (2001). Studying rhythmogenesis of breathing: comparison of in vivo and in vitro models. Trends Neurosci. *24*, 464–472.

Ritter, B., and Zhang, W. (2000). Early postnatal maturation of $GABA_A$-mediated inhibition in the brainstem respiratory rhythm-generating network of the mouse. Eur. J. Neurosci. *12*, 2975–2984.

Rybak, I.A., St. John, W.M., and Paton, F.R. (2001). Models of neuronal bursting behavior: implications for in-vivo versus in-vitro respiratory rhythmogenesis. In Frontiers in Modeling and Control of Breathing: Integration at Molecular, Cellular, and Systems Levels, C.-S. Poon, and H. Kazemi, eds. (New York: Kluwer Academic/Plenum), pp. 159–164.

Shao, X.M., and Feldman, J.L. (1997). Respiratory rhythm generation and synaptic inhibition of expiratory neurons in pre-Botzinger complex: differential roles of glycinergic and GABAergic neural transmission. J. Neurophysiol. *77*, 1853–1860.

Siniscalchi, A., Bonci, A., Mercuri, N.B., and Bernardi, G. (1997). Effects of riluzole on rat cortical neurones: an in vitro electrophysiological study. Br. J. Pharmacol. *120*, 225–230.

Smith, J.C. (1997). Integration of cellular and network mechanisms in mammalian oscillatory motor circuits. Insights from the respiratory oscillator. In Neurons, Networks, and Motor Behavior, P. Stein, S. Grillner, A. Selverston, and D. Stuart, eds. (Cambridge, MA: MIT Press), pp. 97–104.

Smith, J.C., Ellenberger, H.H., Ballanyi, K., Richter, D.W., and Feldman, J.L. (1991). Pre-Bötzinger complex: a brainstem region that may generate respiratory rhythm in mammals. Science *254*, 726–729.

Smith, J.C., Ballanyi, K., and Richter, D.W. (1992). Whole-cell patch-clamp recordings from respiratory neurons in neonatal rat brainstem in vitro. Neurosci. Lett. *134*, 153–156.

Smith, J.C., Butera, R.J., Koshiya, N., Del Negro, C.A., Wilson, C.G., and Johnson, S.M. (2000). Respiratory rhythm generation in neonatal and adult mammals: the hybrid pacemaker-network model. Respir. Physiol. *122*, 131–147.

Song, J.H., Huang, C.S., Nagata, K., Yeh, J.Z., and Narahashi, T. (1997). Differential action of riluzole on tetrodotoxin-sensitive and tetrodotoxin-resistant sodium channels. J. Pharmacol. Exp. Ther. *282*, 707–714.

Stefani, A., Spadoni, F., and Bernardi, G. (1997). Differential inhibition by riluzole, lamotrigine, and phenytoin of sodium and calcium currents in cortical neurons: implications for neuroprotective strategies. Exp. Neurol. *147*, 115–122.

Thoby-Brisson, M., and Ramirez, J.M. (2001). Identification of two types of inspiratory pacemaker neurons in the isolated respiratory neural network of mice. J. Neurophysiol. *86*, 104–112.

Umemiya, M., and Berger, A.J. (1995). Inhibition by riluzole of glycinergic postsynaptic currents in rat hypoglossal motoneurones. Br. J. Pharmacol. *116*, 3227–3230.

Urbani, A., and Belluzzi, O. (2000). Riluzole inhibits the persistent sodium current in mammalian CNS neurons. Eur. J. Neurosci. *12*, 3567–3574.

Wang, H., Stornetta, R.L., Rosin, D.L., and Guyenet, P.G. (2001). Neurokinin-1 receptor-immunoreactive neurons of the ventral respiratory group in the rat. J. Comp. Neurol. *434*, 128–146.

Xu, L., Enyeart, J.A., and Enyeart, J.J. (2001). Neuroprotective agent riluzole dramatically slows inactivation of Kv1.4 potassium channels by a voltage-dependent oxidative mechanism. J. Pharmacol. Exp. Ther. *299*, 227–237.